Journal of the European Ceramic Society **8** (1991) 375–382

The Formation of Phases in the AlN-rich Corner of the Si–Al–O–N System

P. J. Cannard,[a]* Thommy Ekström[b] & R. J. D. Tilley[a]‡

[a] Division of Materials, School of Engineering, University of Wales College of Cardiff, P.O. Box 917, Cardiff CF2 1XH, UK

[b] Department of Inorganic Chemistry, Arrhenius Laboratory, University of Stockholm, S-10691 Stockholm, Sweden

(Received 11 March 1991; accepted 22 April 1991)

Abstract

The reaction of AlN with Al_2O_3, SiO_2 or Si_3N_4 and Al_2O_3 at temperatures of 1820°C and 1950°C and for compositions rich in AlN have been investigated using powder X-ray diffraction, scanning electron microscopy and high-resolution transmission electron microscopy. At 1820°C, Al_2O_3 reacted with AlN to form the non-stoichiometric oxynitride spinel phase ($\approx Al_{23}O_{27}N_5$), whereas samples on the AlN–SiO_2 and AlN–'X-phase' tie-lines did not react. At 1950°C, AlN–Al_2O_3 mixtures reacted to form the 27R aluminium oxynitride polytypoid, AlN–SiO_2 mixtures reacted to form 21R and 27R sialon polytypoids and AlN–'X-phase' mixtures reacted to form the 12H, 21R and 27R sialon polytypoids, all of which possessed a needle-like morphology. Ordered and disordered intergrowths were also observed in the polytypoid crystals but the disordered $2H^{\delta}$ sialon phase was not found.

Die Reaktionen von AlN mit Al_2O_3, SiO_2 oder Si_3N_4 und Al_2O_3 wurden für AlN-reiche Zusammensetzungen bei 1820°C und bei 1950°C mittels Röntgenbeugung, Rasterelektronenmikroskopie und hochauflösender Transmissionselektronenmikroskopie untersucht. Bei 1820°C reagierten Al_2O_3 und AlN unter Bildung der nichtstöchiometrischen Oxinitridspinellphase ($\approx Al_{23}O_{27}N_5$). Proben im Bereich der AlN–SiO_2 und AlN–'X-Phase' Konoden dagegen reagierten nicht. Bei 1950°C bildeten die AlN–Al_2O_3 Mischungen den 27R Aluminiumoxinitridpolytyp. AlN–SiO_2 Mischungen bildeten 21R und 27R Sialonpolytypen und AlN–'X-Phase' Mischungen bildeten 12H, 21R und 27R Sialonpolytypen. Alle diese Polytypen zeigten eine nadelförmige Morphologie. In den polytypen Kristallen wurden ebenso geordnete und ungeordnete Verwachsungen gefunden, die ungeordnete $2H^{\delta}$-Sialonphase konnte jedoch nicht nachgewiesen werden.

On a étudié à l'aide de la diffraction X, de la microscopie électronique à balayage et à transmission à haute résolution, la réactivité de l'AlN avec Al_2O_3, SiO_2 ou Si_3N_4 et Al_2O_3 à des températures égales à 1820 et 1950°C pour des compositions riches en AlN. A 1820°C, Al_2O_3 réagit avec AlN pour former une phase spinelle oxynitrure non-stoechiométrique ($\approx Al_{23}O_{27}N_5$) tandis que les échantillons correspondant aux lignes reliant AlN–SiO_2 et AlN–'phase X' ne réagissent pas. A 1950°C, les mélanges AlN–Al_2O_3 réagissent pour former le polytype d'oxynitrure d'aluminium 27R, les mélanges AlN–SiO_2 conduisent à la formation de polytypes de sialon 21R et 27R et les mélanges d'AlN–'phase X' aux polytypes de sialon 12H, 21R et 27R, présentant tous une morphologies aciculaire. On a également observé des intercroissances ordonnées et désordonnées dans les cristaux de polytypes, la phase sialon désordonnée $2H^{\delta}$ n'étant, quant à elle, pas présente.

1 Introduction

The Si–Al–O–N (sialon) system has been intensively investigated in recent years because many of the phases it contains have engineering applications.[1–5] Of this phase region, the AlN corner has been

* Present address: British Telecom Research Laboratories, Martelsham Heath, Ipswich IP5 7RE, UK.

‡ To whom correspondence should be addressed.

Journal of the European Ceramic Society 0955-2219/91/$3.50

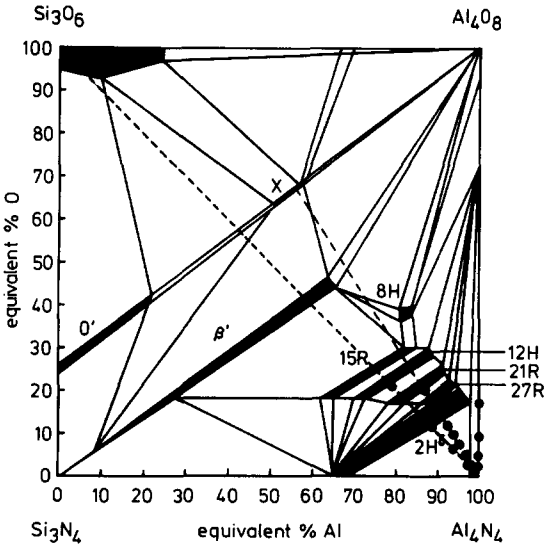

Fig. 1. The reactant ratios for the AlN–Al_2O_3, AlN–SiO_2 and AlN–Al_2O_3–Si_3N_4 series of preparations shown on the Si–Al–O–N pseudoquaternary diagram which also shows the phase relations determined by Jack.[5]

studied the least, although AlN itself has a high thermal conductivity and has potential for use as a ceramic substrate for electronic circuitry. To help clarify the AlN-rich region of the sialon system, the reaction products formed when AlN was reacted with Al_2O_3 alone, SiO_2 alone or SiO_2 and Si_3N_4 along the AlN-'X-phase'[4,6] tie-line, as shown in Fig. 1, were studied by powder X-ray diffraction, scanning electron microscopy and transmission electron microscopy. The results of this investigation are reported in this paper.

2 Experimental

Samples were prepared from the highest purity AlN, SiO_2, Si_3N_4 and Al_2O_3 available (Johnson-Matthey, Royston, Herts, UK). The AlN was stored in an evacuated desiccator to prevent reaction with water vapour to form Al_2O_3. The appropriate quantities of each compound were weighed and well mixed in an agate mortar before being pressed into 13 mm diameter pellets.

Two series of samples were made to study the phases occurring on the AlN–Al_2O_3 and AlN–SiO_2 tie-lines of the Si–Al–O–N phase diagram. These were prepared with ratios of AlN:Al_2O_3 and AlN:SiO_2 of 5:1, 10:1, 20:1 and 50:1. A third series, consisting of mixtures of AlN, Al_2O_3 and Si_3N_4, were designed to produce samples on the AlN–'X-phase' tie-line on the Si–Al–O–N phase diagram, as indicated on Fig. 1. These samples are listed as empirical compositions, e.g. $SiAl_{74.96}O_{2.89}N_{74.37}$

Table 1. Compositions and X-ray diffraction phase analysis at 1950°C

Composition		*Phases present*[a]
5 AlN: 1 Al_2O_3		AlN, (27R)
10 AlN: 1 Al_2O_3		AlN, (27R)
20 AlN: 1 Al_2O_3		AlN, ((27R))
50 AlN: 1 Al_2O_3		AlN
5 AlN: 1 SiO_2		Not fired
10 AlN: 1 SiO_2		27R, 21R, AlN
20 AlN: 1 SiO_2		21R, 27R, AlN
50 AlN: 1 SiO_2		AlN, polytypoids
$SiAl_{74.96}O_{2.89}N_{74.37}$	0·99 AlN: 0·01X[b]	AlN, polytypoids
$SiAl_{37.93}O_{2.89}N_{37.33}$	0·98 AlN: 0·02X	AlN, polytypoids
$SiAl_{25.58}O_{2.89}N_{24.99}$	0·97 AlN: 0·03X	AlN, polytypoids
$SiAl_{19.41}O_{2.89}N_{18.81}$	0·96 AlN: 0·04X	polytypoids, AlN
$SiAl_{15.70}O_{2.89}N_{15.11}$	0·95 AlN: 0·05X	polytypoids, AlN
$SiAl_{8.30}O_{2.89}N_{7.70}$	0·90 AlN: 0·10X	27R, (AlN), ((21R))
$SiAl_{5.83}O_{2.89}N_{5.23}$	0·85 AlN: 0·15X	21R, (27R), (AlN)
$SiAl_{4.59}O_{2.89}N_{4.00}$	0·80 AlN: 0·20X	21R
$SiAl_{3.85}O_{2.89}N_{3.26}$	0·75 AlN: 0·25X	21R, 12H
$SiAl_{3.36}O_{2.89}N_{2.77}$	0·70 AlN: 0·30X	21R, 12H

[a] The phases are listed in order of diminishing presence; those present in small or very small amounts are in parentheses or double parentheses respectively. 'Polytypoids' indicates disordered polytypoid structures that could not be precisely characterised.
[b] The composition of the 'X-phase' is given in Refs 4 and 6.

and as the AlN: 'X' ratio in Table 1. All subsequent references in the text refer to these samples as a function of the AlN: 'X' ratio for convenience. The reactant ratios for the preparations are also indicated on the phase diagram in Fig. 1.

The pressed pellets were embedded in powdered BN and heated on graphite trays which were coated with BN to reduce carbon contamination. A graphite-lined furnace with graphite heating elements and a controlled atmosphere capability was used to heat the samples. Details of the two heating cycles used, 1820°C and 1950°C, are given in Table 2. The temperature within the furnace was monitored automatically with thermocouples and manually using an optical pyrometer.

Powder X-ray diffraction was carried out using IRD XDC 700 and IRD XDC 1000 Hägg–Guinier focusing cameras employing strictly monochromatic Cu$K_{\alpha 1}$ radiation and KCl ($a_0 = 0{\cdot}62923$ nm at 25°C) as an internal standard. The films were measured using a scale graduated in 0·1 mm intervals exposed on the film prior to development. The observed line positions were converted into refined unit-cell dimensions via least squares programs.[7]

For morphology studies pellets were fractured to reveal fresh internal surfaces which were examined in a JEOL 35CF scanning electron microscope equipped with energy and wavelength dispersive

Table 2. Heating cycles 1820°C and 1950°C

Temperature (°C)	*Time (h)*	*Atmosphere*
1 820°C		
20–200	0·5	Vacuum
200–500	1·6	Vacuum
500	0·2	Vacuum
500–700	0·6	1 atm N_2
700–1 100	0·6	1 atm N_2
1 100–1 400	0·5	1 atm N_2
1 400–1 750	0·5	1 atm N_2
1 750–1 820	0·2	1 atm N_2
1 820	5·0	1 atm N_2
1 950°C		
20–200	0·5	Vacuum
200–500	1·6	Vacuum
500	0·2	Vacuum
500–1 820	2·25	1 atm N_2
1 820–1 950	1·1	1 atm N_2
1 950	1·0	1 atm N_2

analysis systems and operated at 21 kV. The fracture surfaces were carbon coated before examination to prevent charging.

Samples for transmission electron microscopy were prepared by crushing a small amount of material under *n*-butanol in an agate mortar. A drop of the resulting suspension was allowed to dry on a copper grid previously covered with a holey carbon film before examination in a JEOL 200CX transmission electron microscope fitted with a high-resolution top entry goniometer stage and operated at 200 kV. The objective lens had a C_s of 1·2 mm and the objective aperture used was 1·8 nm^{-1} in diameter. Through focal series were recorded at increments of either 6 nm or 9 nm defocus. Image simulations were carried out using programs written by Anstis (pers. comm., 1984) which were executed on the Joint Cardiff Computing Services Honeywell DPS-8/70M computer.

3 Results

3.1 X-Ray phase analysis

3.1.1 1820°C Sintering cycle

The AlN–Al_2O_3 samples reacted to give the non-stoichiometric spinel phase $\approx Al_{23}O_{27}N_5$ and excess AlN. There was no trace of Al_2O_3 in the products. None of the AlN–SiO_2 or AlN–Si_3N_4–Al_2O_3 samples reacted to form crystalline phases.

3.1.2 1950°C Sintering cycle

The AlN–Al_2O_3 samples reacted to give the 27R aluminium oxynitride polytypoid together with excess AlN. The X-ray powder photograph of the 5AlN:1Al_2O_3 preparation contained a few extra weak lines besides those of the 27R aluminium oxynitride polytypoid and AlN which could not be attributed to any of the known phases in the system. There was no Al_2O_3 or $\approx Al_{23}O_{27}N_5$ present. These results are summarised in Table 1.

The AlN–SiO_2 samples reacted to form the sialon polytypoids 21R and 27R. Excess AlN was also present. These results are summarised in Table 1.

In the AlN–Si_3N_4–Al_2O_3 system the AlN:0·01 'X' to 0·95AlN:0·05 'X' samples contained both AlN and traces of the 27R and 21R sialon polytypoids. The amount of the polytypoids increased as the AlN content of the samples fell until, in the 0·80AlN:0·20 'X' sample, only the 21R sialon polytypoid was present. In the 0·75AlN:0·25 'X' and 0·70AlN:0·30 'X' samples the 21R sialon polytype was present together with the 12H sialon polytypoid. There was no trace of Si_2N_4 or Al_2O_3 on any of the films. These results are summarised in Table 1.

3.2 Scanning electron microscopy

3.2.1 1820°C Samples

The only sample examined was 5AlN:1Al_2O_3 as samples in the AlN–SiO_2 and AlN–Si_3N_4–Al_2O_3 systems had not reacted. The microstructure of the sample showed many small equiaxed grains together with some larger grains as shown in Fig. 2. The AlN grains could not be distinguished from grains of the non-stoichiometric spinel phase $\approx Al_{23}O_{27}N_5$ by morphology or by EDAX analysis.

3.2.2 1950°C Samples

The sample 5AlN:1Al_2O_3 clearly showed two types

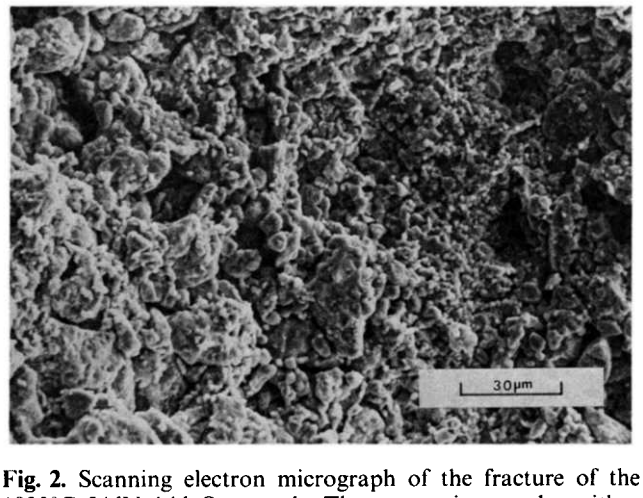

Fig. 2. Scanning electron micrograph of the fracture of the 1820°C 5AlN:1Al_2O_3 sample. The texture is granular with a substantial number of smaller equiaxed grains and a few larger grains. These grains are a mixture of AlN and AlON.

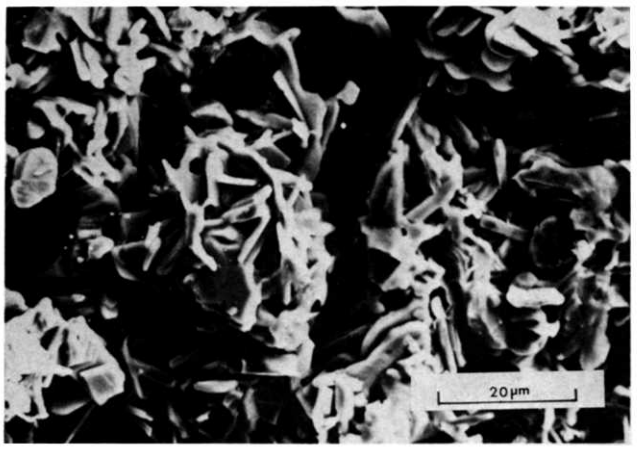

Fig. 3. Scanning electron micrograph of the fracture surface of the 1950°C AlN:1Al_2O_3 sample. Two morphologies are clearly visible, needle-like and equiaxed.

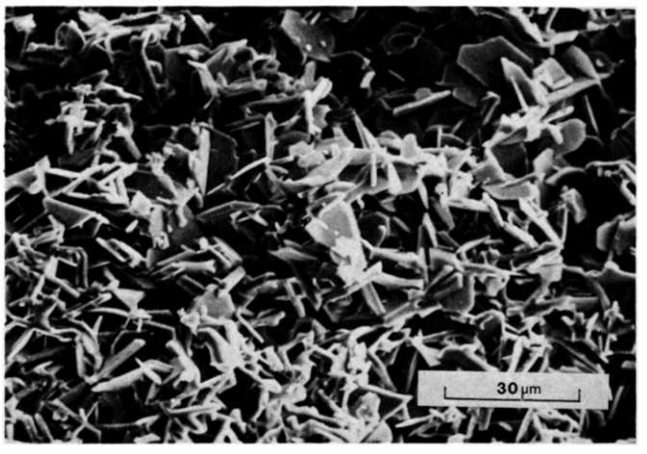

Fig. 4. Scanning electron micrograph of the fracture surface of the 1950°C 0·85AlN:0·15X sample showing the morphology expected with sialon polytypoids. A series of interlocking needles binds the specimen together with some 'plate-like' AlN grains dispersed amongst them.

of morphology, needle-like and equiaxed/plate-like, illustrated in Fig. 3. Comparison with the literature[8-10] makes it reasonable to suppose that the needle-like grains are 27R aluminium oxynitride polytypoid, and that the equiaxed or plate-like grains are AlN.

The microstructure of the 0·85AlN:0·15 'X' sample, which was typical of the type of microstructure found when AlN and sialon polytypoids coexist, is shown in Fig. 4. This shows a series of interlocking needles with some plate-like grains dispersed amongst them. EDAX analysis of the plate-like grains showed them to be AlN, while the needles were shown to be sialon polytypoids.

3.3 Transmission electron microscopy of polytypoids

Electron diffraction patterns from polytypoid crystal fragments could be interpreted using existing data. The results of the phase analysis are shown in Table 3. Although crystal fragments of the polytypes were generally well ordered, two different forms of disorder microstructure were found. In samples close to the AlN corner of the phase diagram biphasic AlN/27R sialon polytypoid crystal fragments were sometimes observed. Typical of these is the example shown in Fig. 5, found in the 0·90 AlN:0·10 'X' sample. In samples from other parts of the phase region disorder usually took the form of intergrown layers of different thicknesses. As an example, Fig. 6, taken from the 10AlN:1Al_2O_3 preparation, shows a 27R aluminium oxynitride polytypoid with one extra AlN layer occasionally inserted between the $AlO_{1.5}$ layers, generating coherently intergrown slabs of the 20H aluminium oxynitride polytypoid within the 27R matrix. This polytype has not previously been observed in the AlN–Al_2O_3 system.

Ordered intergrowths of polytypoid structures were also observed occasionally. As an example Fig. 7 shows a fragment of a crystal found in the 0·70AlN:0·30 'X' preparation which is made up of an ordered intergrowth of 15R and 21R sialon polytypoids. To confirm this interpretation of the micrograph, images were calculated for a 5, 7, 5, 7 stacking sequence, employing the atomic coordinates listed in Table 4, which derived from the structural data of Thompson.[11] Image simulations showing matching at −42·5 nm and −62·5 nm, inset on Fig. 7(B) and (C), confirm the interpretation. The fragment also contains a defect consisting of an intergrown slab of 21R sialon polytypoid structure.

Table 3. Electron microscope phase analysis

Sample[a]	*12H*	*21R*	*27R*	*Disordered*	*Total*
10 AlN: 1 Al_2O_3	—	—	3	—	3
0·90 AlN: 0·10X	—	—	7	—	7
0·85 AlN: 0·15X	—	1	3	—	4
0·70 AlN: 0·30X	6	—	—	1	7

[a] The phases are listed in order of diminishing presence; those present in small or very small amounts are in parentheses or double parentheses respectively. 'Polytypoids' indicates disordered polytypoid structures that could not be precisely characterised.

4 Discussion

The results found for the AlN–Al_2O_3 preparations are by and large in agreement with the phase equilibrium data reported by McCauley & Corbin.[12] At 1820°C only the AlN–Al_2O_3 mixtures reacted, and produced the non-stoichiometric spinel phase $\approx Al_{23}O_{27}N_5$. At 1950°C $\approx Al_{23}O_{27}N_5$ gave way to the needle-like 27R aluminium oxynitride

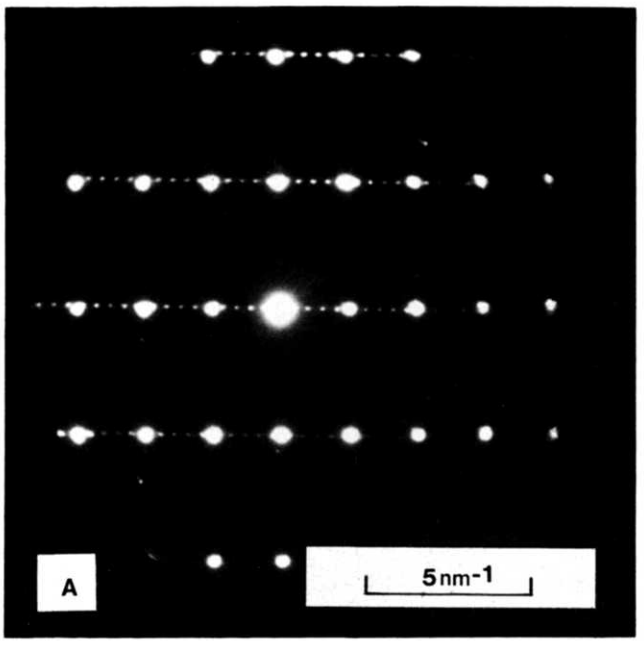

Fig. 5. Fragment taken from the 0·90AlN:0·1 'X' sample. A, the electron diffraction pattern is a superposition of a 2H AlN diffraction pattern and a 27R sialon polytypoid diffraction pattern. B, the electron micrograph reveals two regions, AlN and 27R sialon polytypoid.

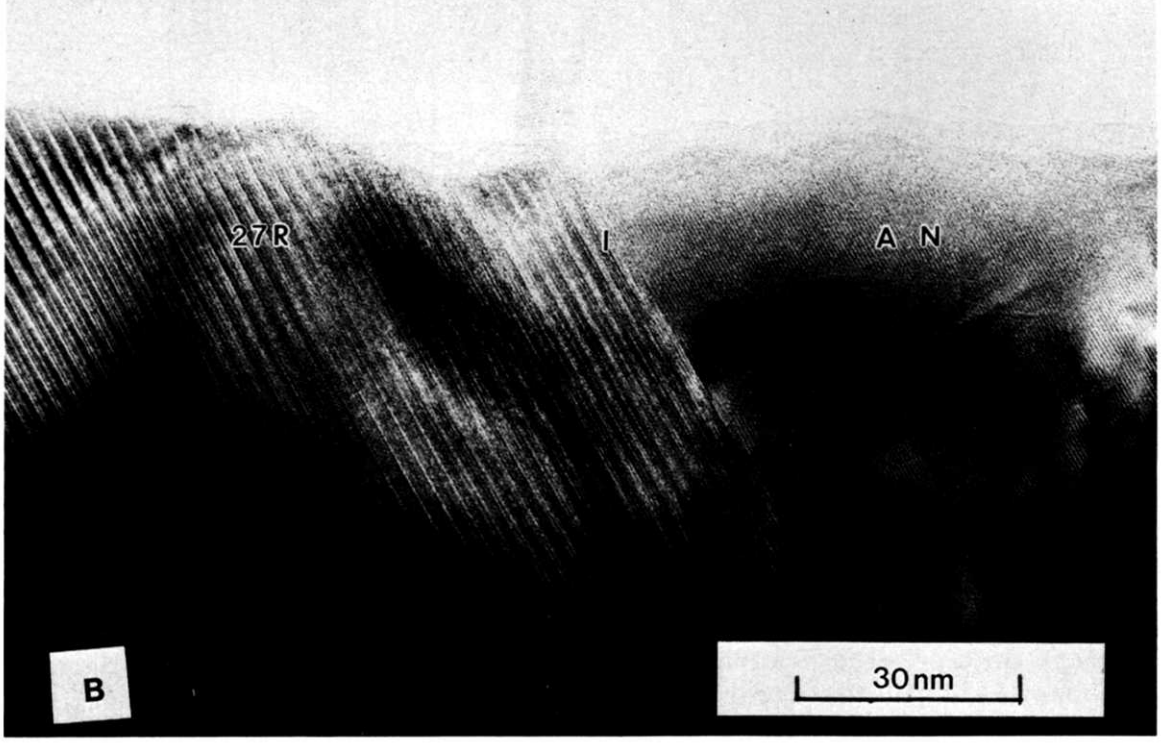

polytypoid. The phase relations suggested that the products of sintering the 10, 20 and 50AlN:1Al_2O_3 samples would be AlN and 27R polytype, while the 5AlN:1Al_2O_3 sample should yield 27R AlN polytype and $\approx Al_{23}O_{27}N_5$. However, only AlN and the 27R AlN polytype were found by X-ray diffraction in all of the samples fired at 1950°C. This would indicate a slight loss of oxygen during sintering, moving the composition of the 5AlN:1Al_2O_3 sample into the AlN + 27R AlN polytype region of the phase diagram. The use of densifying agents to reduce porosity is likely to reduce this loss significantly at higher reaction temperatures and should result in samples in agreement with the phase diagram.

The sequence of phases found in the AlN–SiO_2 and AlN–Si_3N_4–Al_2O_3 samples were in good agreement with the phase data presented by Jack,[5] although the ordered intergrowth of the 15R/21R sialon polytypoid structures has not been observed as a bulk phase before and a $2H^{\delta}$ sialon phase region was not found. This latter phase region is of some interest. Based upon the structures of other polytypes[11,13] the structure of the 27R phase can be

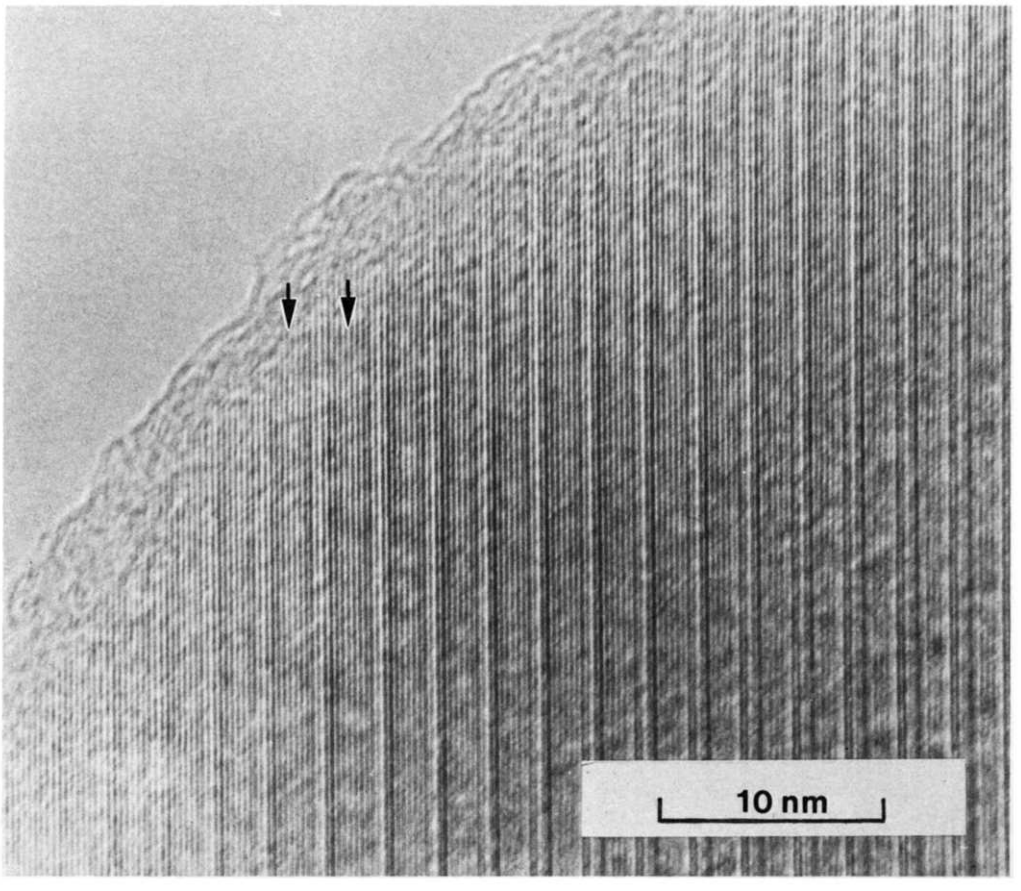

Fig. 6. Electron micrograph of a crystal fragment taken from the 10AlN:1Al_2O_3 sample. The bulk structure corresponds to a 27R aluminium oxynitride polytypoid. Arrowed are two adjacent slabs of ten layers which are an intergrowth of 20H aluminium oxynitride polytypoid.

considered to be ordered intergrowths of the AlN (wurtzite) structure and the Al_2O_3 (corundum) structure. The composition range between AlN and the 27R polytype phase could be envisaged either as a classical two-phase region or as a non-stoichiometric phase region in which the corundum-type lamellae become more and more dilute in the AlN matrix, in a similar way to that found in the analogous system $ZnO–In_2O_3$.[14] The evidence presented in Fig. 5 shows that the AlN 2H structure coexists with the 27R polytype structure, even in single grains. Thus under the conditions of these preparations a definite two-phase equilibrium occurs. The disordered $2H^{\delta}$ phase shown on Fig. 1, which could be a non-stoichiometric region containing disordered lamellae of corundum structure, may possibly represent a form found at higher temperatures.

The sequence of phases found in the $AlN–Al_2O_3$, $AlN–SiO_2$ and $AlN–Si_3N_4–Al_2O_3$ samples is similar, but the polytypoid structures which occur are different. At 1950°C the 12H, 21R and 27R sialon polytypoids were readily formed in the $AlN–SiO_2$ and $AlN–Si_3N_4–Al_2O_3$ systems, whereas only the 27R AlN polytype was formed in the Al–O–N system. The other aluminium oxynitride polytypoids form at progressively higher temperatures, viz. 27R: 1920°C, 21R: 2000°C, 12H: 2050°C.[12]

The relative stabilities of the polytype phases will depend upon a number of factors and has been investigated theoretically by Price & Yeomans[15] and Angel *et al.*[16] The Al–O–N polytypes differ from the sialon polytypes in that there are no Si atoms present and higher ratios of oxygen atoms with respect to nitrogen atoms need to be incorporated into the structure to preserve the charge balance. The presence of this additional oxygen will induce an alternative strain energy, internal energy and interfacial energy compared to the equivalent sialon polytype phase. From the phase data in Refs 5 and 12 it seems that higher temperatures are needed in the $AlN–Al_2O_3$ system to offset the lack of Si, which seems to compensate for the interactions due to the MO layers in these structures. It is interesting to note that 8H AlN polytype has only been reported in the Si–Al–O–N system and not at all in the Al–O–N system, possibly due to the fact that the AlO_6 octahedra are now too close together for the lattice

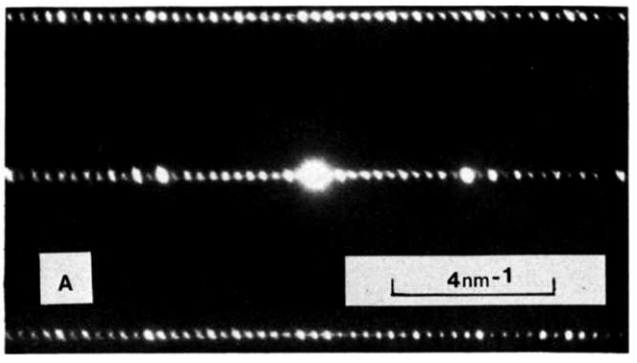

Fig. 7. A, electron diffraction pattern, and B–D, micrographs, of a fragment taken from the 0·70 AlN:0·30 'X' sample. B Shows that the crystal is made up of alternating blocks of five and seven metal layers. Image simulations inset on the higher magnification prints, C, at −42·5 nm and, D, at −62·5 nm confirm that the crystal consists of a parallel intergrowth of 15R and 21R sialon polytypoid structures. A fault consisting of a slab of 21R sialon polytypoid structure is also present.

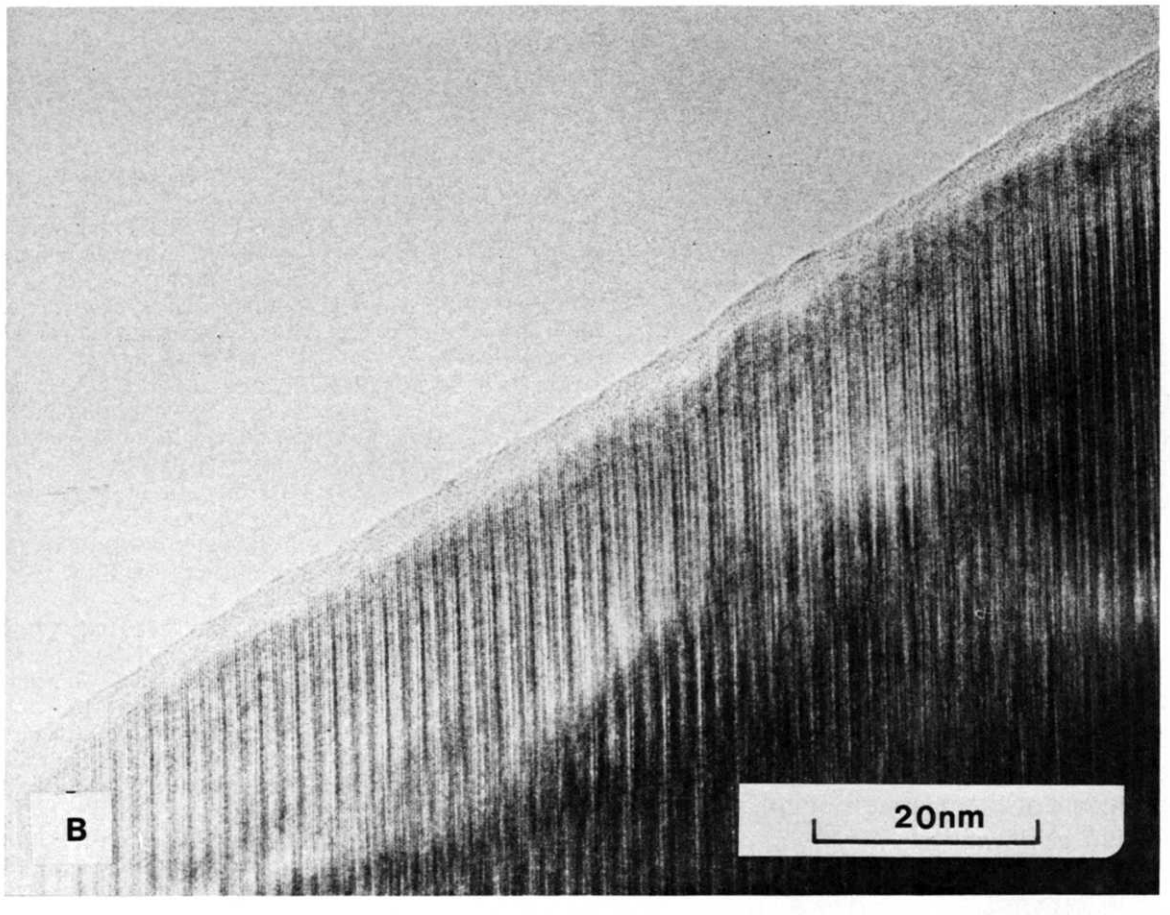

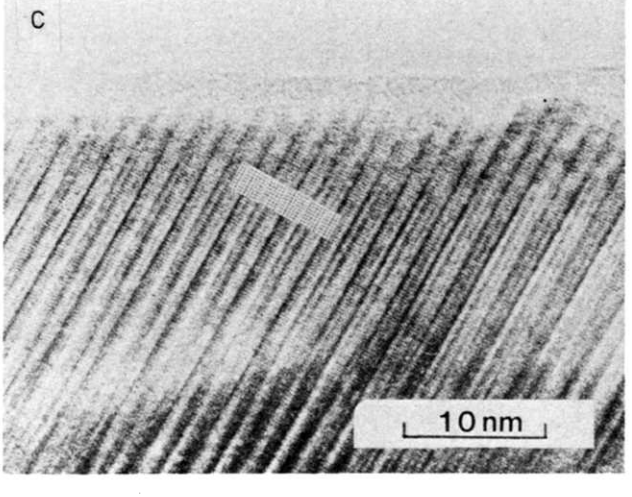

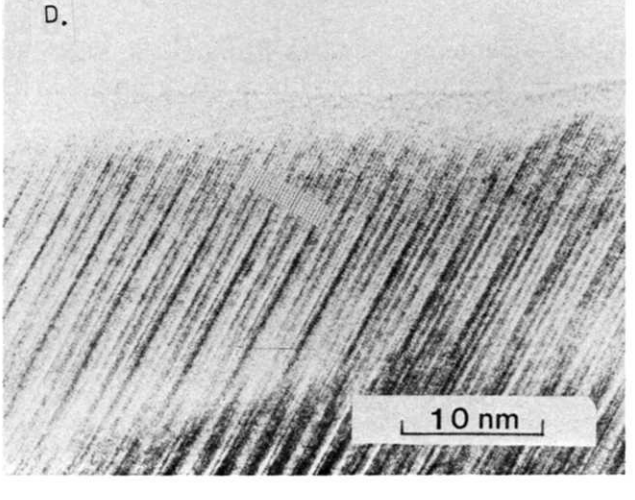

Table 4. Atomic parameters used for simulating the 15R/21R intergrowth structure

Atom	*x*	*y*	*z*
Al/Si	0	0	0
Al/Si	0	0	0·057 8
Al/Si	0	0	0·111 5
Al/Si	0	0	0·170 3
Al/Si	0	0	0·224 5
Al/Si	0	0	0·278 6
Al/Si	0	0	0·472 9
Al/Si	0	0	0·530 7
Al/Si	0	0	0·584 9
Al/Si	0	0	0·638 6
Al/Si	0	0	0·697 4
Al/Si	0	0	0·751 5
O	0	0	0·296 2
O	0	0	0·455 1
O	0	0	0·769 1
O	0	0	0·982 2
N	0	0	0·027 6
N	0	0	0·077 5
N	0	0	0·142 8
N	0	0	0·190 0
N	0	0	0·244 1
N	0	0	0·500 5
N	0	0	0·550 4
N	0	0	0·604 5
N	0	0	0·669 8
N	0	0	0.717 1

$a = 0{\cdot}303$ nm, $c = 10{\cdot}122$ nm. Rhombohedral symmetry with equivalent positions as follows:

$$+2/3\ 1/3\ 1/3 \quad \text{and} \quad +1/3\ 2/3\ 2/3$$

All atoms given Debye–Waller factors = 0·005 nm^2 and an occupancy of 1·0.

distortions to be accommodated in the absence of Si. Thus small local changes in stoichiometry could be the reason why the 20H and 21R/15R intergrowths reported here for the first time were observed. Clearly further studies of the relative stabilities of the polytypes would be of interest.

Acknowledgements

PJC is indebted to Sandvik Ltd and the SERC for financial support. The authors are grateful to Dr David Jack for his interest and encouragement during the course of this study.

References

1. Oyama, Y. & Kamigaito, O., Solid solubility of some oxides in silicon nitride. *Jpn J. Appl. Phys.*, **10** (1971) 1637–42.
2. Oyama, Y., Solid solution in the ternary system, silicon nitride–aluminium nitride–aluminium oxide. *Jpn J. Appl. Phys.*, **11** (1972) 760–1.
3. Jack, K. H. & Wilson, W. I., Ceramics based on the Si–Al–O–N and related systems. *Nature, Phys. Sci.*, **238** (1972) 28–9.
4. Gauckler, L. J., Lukas, H. L. & Petzow, G., Contribution to the phase diagram Si_3N_4–AlN–Al_2O_3–SiO_2. *J. Amer. Ceram. Soc.*, **58** (1975) 346–7.
5. Jack, K. H., Sialons and related nitrogen ceramics. *J. Mater. Sci.*, **11** (1976) 1135–58.
6. Thompson, D. P. & Korgul, P., Sialon X-phase. In *Progress in Nitrogen Ceramics*, ed. F. L. Riley. Martinus Nijhoff, The Netherlands, 1983, pp. 375–80.
7. Brandt, B. G. & Nord, A. G., A set of crystallographic programs for an IBM 360/75 computer. Chem Commun. Univ. Stockholm, No. 5, 1970.
8. Van Tendeloo, G., Faber, K. T. & Thomas, G., Characterisation of aluminium nitride ceramics containing long-period polytypes. *J. Mater. Sci.*, **18** (1983) 525–32.
9. Krishnan, K. M., Rai, R. S., Thomas, G., Corbin, N. D. & McCauley, J. W., Characterisation of long-period polytypoid structures in the alumina–aluminium nitride system. *Mater. Res. Soc. Symp. Proc.*, **60** (1986) 211–18.
10. Clarke, D. R. & Shaw, T. M., Polytypism in magnesium sialon. *Mater. Sci. Res.*, **11** (1978) 589–96.
11. Thompson, D. P., The crystal structures of 8H and 15R sialon polytypes. In *Nitrogen Ceramics*, ed. F. L. Riley. 1978, pp. 129–35.
12. McCauley, J. W. & Corbin, N. D., High-temperature reactions and structures in the Al_2O_3–AlN system. In *Progress in Nitrogen Ceramics*, ed. F. L. Riley. Martinus Nijhoff, Leyden, The Netherlands, 1983, pp. 111–18.
13. Bando, Y., Mitomo, M., Kitami, Y. & Izumi, F., Structure and composition analysis of silicon aluminium oxynitride polytypes by combined use of structure imaging and microanalysis. *J. Microsc.*, **142** (1986) 235–46.
14. Cannard, P. J. & Tilley, R. J. D., New intergrowth phases in the zinc oxide–indium oxide system. *J. Solid State Chem.*, **73** (1988) 418–26.
15. Price, G. D. & Yeomans, J., The application of the ANNNI model to polytypic behaviour. *Acta Crystallogr.*, **B40** (1984) 448–54.
16. Angel, R. J., Price, G. D. & Yeomans, J., The energetics of polytype structures: Further applications of the ANNNI model. *Acta Crystallogr.*, **B41** (1985) 310–19.

Journal of the European Ceramic Society **8** (1991) 383–388

Thermal Evolution of Fe_2O_3–TiO_2 Sol–Gel Thin Films

P. Colombo, M. Guglielmi

Dipartimento di Ingegneria Meccanica, Sezione Materiali, Università di Padova, via Marzolo 9, 35131 Padova, Italy

&

S. Enzo

Dipartimento di Chimica Fisica, Unità Consorzio INFM, Calla Larga S. Marta 2137, 30123 Venezia, Italy

(Received 16 April 1991; accepted 21 May 1991)

Abstract

Fe_2O_3–TiO_2 thin films were deposited on silica glass slides using three sol–gel solutions containing Ti-butoxide and different iron oxide precursors. The thermal evolution of the coatings was followed by DTA–TGA and XRD from 200 to 1000°C. All the iron-containing samples were amorphous up to 700°C, when a phase separation between iron and titanium oxides was evidenced by the presence of crystalline Fe_2O_3. Above that temperature a titanate compound (pseudobrookite) formed according to the equilibrium phase diagram. The use of different precursors did not affect the thermal evolution and all the different samples exhibited the same trend.

Auf SiO_2-Glasplättchen wurden mittels dreier Sol–Gel–Lösungen aus Ti-Butoxid und unterschiedlichen Eisenoxidprecursoren dünne Fe_2O_3–TiO_2-Schichten erzeugt. Das thermische Verhalten der Schichten wurde im Temperaturbereich von 200°C bis 1000°C mit Hilfe der DTA, TGA und XRD untersucht. Bis 700°C waren alle eisenhaltigen Proben amorph. Bei 700°C fand eine Phasentrennung zwischen den Oxiden statt, was durch das Auftreten kristallinen Fe_2O_3 nachgewiesen werden konnte. Über dieser Temperatur bildete sich gemäß dem Phasendiagramm eine Titanat-Verbindung (Pseudobrookit). Die Verwendung verschiedener Precursor hatte keinen Einfluß auf das thermische Verhalten; alle Proben zeigten die gleiche Tendenz.

On a déposé des films fins de Fe_2O_3–TiO_2 sur des lamelles de silice en utilisant trois solutions sol–gel différentes, contenant du butylate de titane et différents précurseurs d'oxyde de fer. L'évolution thermique des couches minces a été suivie par ATD–ATG et XRD de 200 à 1000°C. Tous les échantillons contenant du fer sont amorphes jusqu'à 700°C, tandis qu'une séparation de phase entre le fer et les oxydes de titane est mise en évidence par la présence de Fe_2O_3 cristallin. Aux températures plus élevées, il se forme un composé à base de titane (pseudobrookite), conformément au diagramme de phase à l'équilibre. L'utilisation de différents précurseurs n'affecte pas l'évolution thermique, tous les échantillons présentent la même tendance.

1 Introduction

Oxide coatings based on the TiO_2–Fe_2O_3 system may be deposited on flat glass to give optical properties interesting for practical applications. As reported by Schroeder[1] the UV absorption edge of TiO_2 can be shifted at higher wavelengths, without decreasing its steepness, by admixing other metal alkoxides, such as those of Ni, Fe or Co. In these combinations the formations of compounds (titanates) are said to be responsible for the change of the characteristic absorption of the pure metal oxides.

In this sense TiO_2–Fe_2O_3 coatings could be applied on flat glass to increase its protection against near-UV radiation without decreasing significantly the visible transmittance.

In a previous paper[2] TiO_2–Fe_2O_3 thin films were deposited on soda-lime glass slides from different solutions and transmittance curves were studied as a

Journal of the European Ceramic Society 0955-2219/91/$3.50

function of film thickness. The same solutions were also used to prepare bulk gels which were studied from the point of view of crystallization behaviour[3] and by Mössbauer spectroscopy to try to elucidate the structural evolution upon heating.[4]

In this work the thermal evolution of thin TiO_2 and TiO_2–Fe_2O_3 films deposited on silica slides was studied between 200 and 1000°C, following their weight loss, thickness shrinkage and crystallization. A comparison between films and previously studied powders is presented.

2 Experimental

Three solutions for the preparation of Fe_2O_3–TiO_2 gels with a Fe_2O_3/TiO_2 molar ratio of 0·15 were prepared using three different precursors for iron oxide: (I) $Fe(C_5H_7O_2)_3$; (II) $Fe(NO_3)_3 . 9H_2O$; (III) $Fe(OC_2H_5)_3$; $Ti(OC_4H_9)_4$ was used as precursor for TiO_2. It was dissolved in ethanol with acetylacetone (AcAc/TiBut molar ratio = 0·5) and the correct amount of iron precursor was added. Two other solutions were also prepared by mixing $Ti(OC_4H_9)_4$ and ethanol with acetylacetone (AcAc/TiBut molar ratio = 0·5) (IVa) and without acetylacetone (IVb); all the solutions had a concentration of 10 g of oxides per litre. Silica glass slides were used as substrate. In order to get a reasonable thickness for the analyses (about 2000 Å), a multi-dipping coating procedure was adopted. After each deposition and before the next one the coated slides were treated for 15 min at 200°C.

The samples were then fired with a 15-h-long, 100°C step schedule from 200 to 1000°C introducing them directly into the hot furnace. After each step the thickness of the coatings was measured by a stylus apparatus. The thermal transformations of the films were followed by TGA and DTA and the crystallinity was detected by X-ray diffraction (35 kV, 30 mA, CuK_α radiation) with a conventional θ-2θ Bragg–Brentano goniometer.

Selected angular ranges were step-scanned several times until reaching a satisfactory signal-to-noise ratio. The instrumental function was determined with a α-SiO_2 sample free from crystal size and lattice disorder. For the microstructural characterization an improved profile fitting method[5] using a pseudo-Voigt representation for the line profiles was used.

3 Results

3.1 Thermal analyses

The analyses were performed on powders obtained from unheated gelled films. In Figs 1–4 are reported the curves for the different samples, obtained using the same amount of powder.

The DTA data showed for all the systems containing acetylacetone a complex exothermic pattern in the temperature range 150–400°C, which was almost completely absent in sample IVb. It can be noticed that weight losses were associated with each exothermic peak.

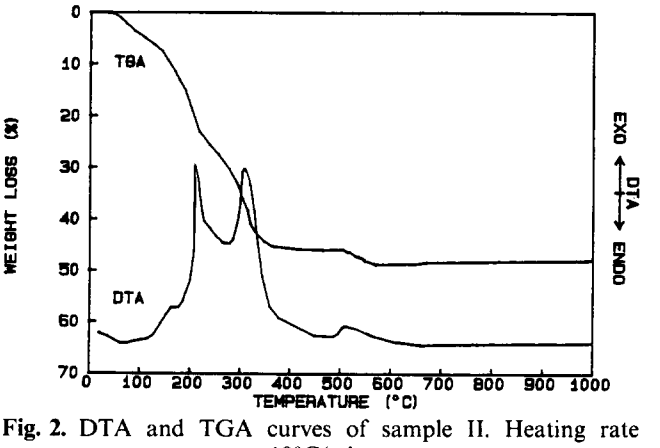

Fig. 2. DTA and TGA curves of sample II. Heating rate 10°C/min.

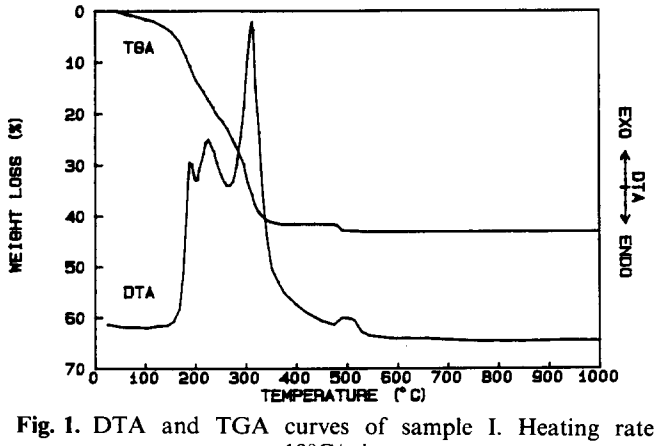

Fig. 1. DTA and TGA curves of sample I. Heating rate 10°C/min.

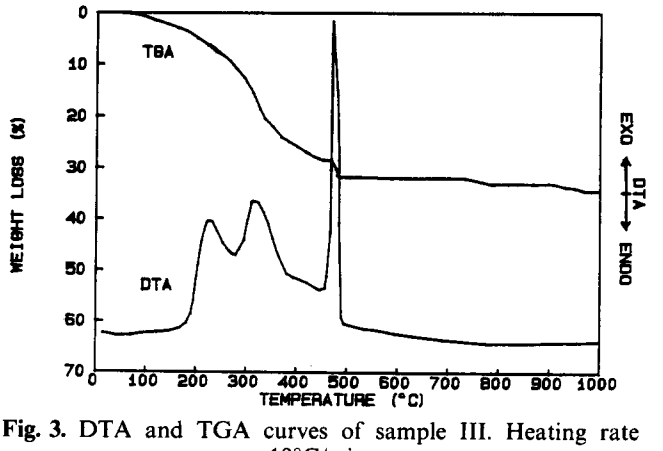

Fig. 3. DTA and TGA curves of sample III. Heating rate 10°C/min.

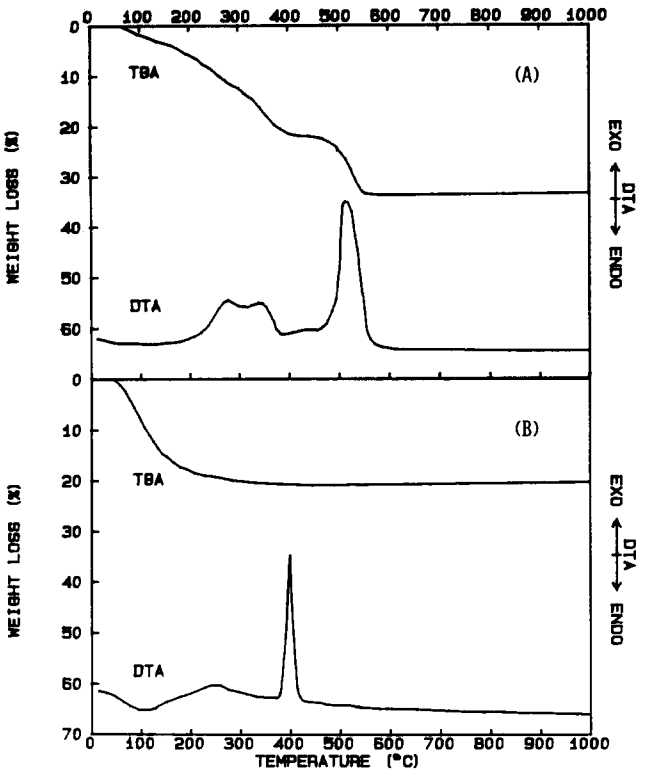

Fig. 4. DTA and TGA curves of sample IVa (a) and IVb (b). Heating rate 10°C/min.

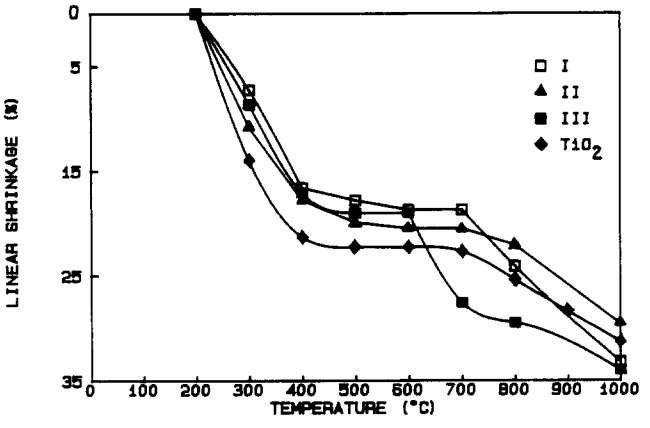

Fig. 5. Linear shrinkages of different samples.

An exothermic effect at around 500°C was also exhibited by all acetylacetone containing samples, whose intensity and sharpness varied from case to case. It was associated with a weight loss. A different exothermic peak was present in both samples IVa and IVb (particularly in IVb) not related to any weight loss, due to the crystallization of anatase.

3.2 Film thickness and shrinkage

Film thicknesses ranged from 3000 Å, for samples at 200°C, to 1500 Å, after heating at 1000°C. The shrinkages are reported in Fig. 5. All the four different systems exhibited the same behaviour.

In the temperature range 200–400°C there was the maximum contraction (about 20%), clearly associated with the weight losses previously described. Between 400 and 600°C there was a very slight contraction which does not seem proportional to the weight losses recorded for the different samples. In this range of temperatures sample I, for instance, had a 1·4% contraction and a 44% weight loss (at 505°C), while sample II had a 2·4% contraction and a 5% weight loss (at 510°C). For temperatures over 600°C all the samples showed an average contraction of 10–15%, although there were not any weight losses.

3.3 X-ray diffraction

As described in the experimental section, the samples were fired from 200 to 1000°C at steps of 100°C, and analysed after each step. Samples I, II and III, which contain iron oxide, showed the same trend and did not present any crystallization phenomena until 700°C, when haematite (α-Fe_2O_3) and rutile (TiO_2) appeared. At 800°C, due to a solid state reaction, pseudobrookite (Fe_2TiO_5) formed and haematite disappeared. A typical set of XRD patterns, relative to sample III, is shown in Fig. 6. In TiO_2 samples anatase and rutile appeared at 400°C and 900°C respectively.

The average crystallite sizes were calculated using the Scherrer equation[6] and are reported in Table 1. In Table 2 are reported semiquantitative data for the

Table 1. Average crystallite size

Temperature (°C)	*I*			*II*			*III*			*IVa*	
	H	*PB*	*R*	*H*	*PB*	*R*	*H*	*PB*	*R*	*A*	*R*
400	—	—	—	—	—	—	—	—	—	163	—
500	—	—	—	—	—	—	—	—	—	166	—
600	—	—	—	—	—	—	—	—	—	236	—
700	250	—	115	180	—	136	200	—	129	320	—
800	—	298	198	—	342	183	—	233	271	381	—
900	nm	nm	nm	nm	nm	nm	nm	nm	nm	432	579
1000	—	352	420	—	276	377	—	342	382	511	543

H, haematite (α-Fe_2O_3); PB, pseudobrookite (Fe_2TiO_5); R, rutile (TiO_2); A, anatase (TiO_2); nm = not measured.